Advances in Materials Physics and Chemistry, 2015, 5, 22-30
Published Online January 2015 in SciRes. http://www.scirp.org/journal/ampc
http://dx.doi.org/10.4236/ampc.2015.51004

Fabrication and Characterization of Graphene Based Nanocomposite for Electrical Properties

Manoj Kumar Pati[1*], Puspalata Pattojoshi[1], Gouri Sankar Roy[2]

[1]Department of Physics, KIIT University, Odisha, India
[2]Department of Physics, College of Engineering and Technology, Bhubaneswar, Odisha, India
Email: [*]manojkumarpati43@gmail.com

Received 3 December 2014; accepted 16 December 2014; published 15 January 2015

Abstract

In the present study, we have described the synthesis of acid functionalized graphene (GE) which was grafted to chitosan (CH) by first reacting the oxidized GE with thionyl chloride to form acyl-chlorinated GE. This product was subsequently dispersed in chitosan and covalently grafted to form GE-chitosan. GE-chitosan was further grafted onto poly(anthranilic acid) (PAA) by free radical polymerization conditions, to yield GE-g-chitosan-g-PAA for our investigations. The structure of GE-CH-PAA composites was characterized by X-ray diffraction (XRD) pattern, Fourier transform infrared (FTIR) spectroscopy, thermo gravimetric analysis (TGA), cyclovoltammetrie (CV) and transmission electron microscopy (TEM). XRD report suggested the strongly crystalline character of the specimen prepared. The performance of cycle voltammeter was attributed to the GE-CH-PAA, which provided a large number of active sites and good electrical conductivity. Experimental results suggested that nanocomposites could be combined together for industrial applications.

Keywords

Graphene, Chitosan, Poly(Anthranilic Acid), Electrical Conductivity

1. Introduction

Graphite is a 2-dimensional carbon material which is naturally abundant. In graphite, sp^2 hybridized carbons are covalently bonded in hexagonal manner forming individual sheets called “grapheme” and these sheets are bound together by van der Waals forces. Graphite has been used in many industrial applications such as lubricants and

[*]Corresponding author.

How to cite this paper: Pati, M.K., Pattojoshi, P. and Roy, G.S. (2015) Fabrication and Characterization of Graphene Based Nanocomposite for Electrical Properties. *Advances in Materials Physics and Chemistry*, **5**, 22-30.
http://dx.doi.org/10.4236/ampc.2015.51004

high temperature gaskets [1]-[3]. To date, the exfoliation of graphite to graphene (GE) and its incorporation into polymers have been rarely reported. Low solubility, strong interaction and small spacing between stacked graphene planes make it nearly impossible to achieve a fully separated state of graphene by pure mechanical mixing with solvents/polymers. Many attempts have been made to exfoliate graphite sheets using intercalation with alkali metals or exposing them to strong acidic conditions [4]-[6]. Expansion of layer spacing takes place via heat treatment [7]-[10] or alternatively, by exposure to microwave radiation followed by mechanical grinding [10]-[12]. These expanded graphite platelets can be incorporated into polymers via solvent mixing [13]-[16], *in-situ* polymerization [17]-[20], or coating onto polymer particles followed by melt processing [21]. Expanded graphite yielded relatively better dispersion than un-intercalated graphite. Still, complete exfoliation to the level of single atomic sheets was not attained using these approaches. The thickness of the resulting layers is typically 10 - 100 nm which is much greater than single graphene sheet thickness (0.34 nm) [22] [23].

Graphene nanosheets have very promising electronic properties and various synthesis methods have been developed to make utilization of graphene viable. So far, the use of graphene has covered a broad range of areas. Moreover, graphene has attracted the significant attention for energy storage and conversion. Its potential applications in super capacitors [24], lithium-ion batteries [25], lithium-sulfur batteries [26], and the latest developed lithium-air batteries have also been intensively investigated.

Chitosan (CH), a N-deacetylated derivative of chitin, consists of 2-amino-2-deoxy (1-4)-*β*-D-glucopyranose residue (or D-glucosamine units) and is derived from the partial alkaline deacetylation of chitin. Chitin, the precursor of chitosan, is a cellulosic type biopolymer which is widely distributed in nature, especially in the shell of crustaceans, the cell wall of fungi and exoskeleton of insects. Chitosan has been developed as a new bioactive material since it possesses various biomedical activities [27] [28]. Chitosan's solubility and poor mechanical properties limit its widespread applications. Chitosan is insoluble in water but dissolves in aqueous solutions of organic acids like acetic, formic and citric acids. It is attractive due to its biocompatibility, biodegradability, nontoxicity and exhibits excellent film-forming ability. It can be used as a modifier due to the abundance of $-NH_2$ and -OH functional groups which renders it ideal for a variety of chemical modifications. Although some successful carbon nanotube chitosan based nanocomposites have been reported, to our knowledge, most of them were obtained by non-covalent interactions such as blending [29], layer-by-layer self-assembly [30], surface deposition and crosslinking and electrochemical deposition on the surface of GE [31]. Covalent GE to chitosan will produce more stable composite, prevent leaching of materials during applications, improve hydrophilicity depending on the functionality introduced and ensure long term stability of GE in the media.

In this study, we have taken advantage of the existence of some of the free amino groups on chitosan, to graft functionalized GE (**Figure 1**), which were further grafted to PAA, and to yield GE-chitosan-PAA. The chemical modifications were confirmed using XRD, FTIR, TGA, TEM and CV measurements. With proper aniline content, the GE-chitosan-PAA nanocomposite is found to exhibit improved capacitance suitable for charge storage applications.

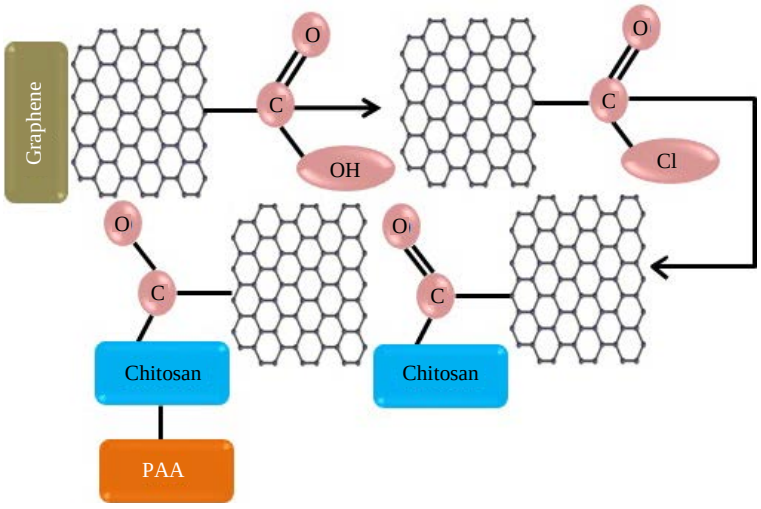

Figure 1. The reaction scheme for synthesis of GE-chitosan-PAA.

2. Experimental Method

2.1. Materials

Poly(anthranilic acid, PAA) was purchased from sigma Aldrich. Graphene used in this work was purchased from Sigma-Aldrich. Other reagents like ammonium persulfate (APS), hydrochloric, sulfuric and nitric acid (Sigma Chemicals) were of analytical grade.

2.2. Synthesis of Functionalized Graphene

Functionalized graphene (FG) was synthesized as described in the recent literature [32]. Typically, GE was reacted with H_2SO_4:HNO_3 (3:1), then tip sonicated for 30 minutes using an ultrasonic processor with amplitude at 30% and 7 s pulse to yield carboxylic acid functionalized GE (GE-COOH). The carboxylic acid group was converted to formyl chloride via reaction with thionyl chloride for 24 h at 75˚C while refluxing. This resulted in functionalized GE which is referred to as GE-COCl. After the reaction was stopped, reaction mixture was cooled before centrifuging and washing to remove excess reactants. Samples were dried overnight at 90˚C and 30 in Hg.

2.3. Synthesis of GE-Chitosan Derivative

During this process, the functionalized GE-COCl (400 mg) was reacted with chitosan (2 g) in 100 mL 2% acetic acid at 75˚C for 24 hours while stirring. After the reaction was stopped, the product was washed three times with 2% acetic acid to remove the unreacted chitosan.

2.4. Synthesis of GE-Chitosan Grafted Derivative

To synthesize GE-chitosan derivative, GE-chitosan (0.1 g) was reacted with $K_2S_2O_8$ (0.02 g) and PAA (6 mL) in 2% acetic acid solution at 75˚C for 2 hours. This product was centrifuged at 20,000 rpm and washed twice with water before drying at 90˚C. This process resulted in the composite product which is referred to as GE-chitosan-PAA.

3. Measurements and Characterization

Following measurements were carried out to confirm chemical modifications of graphene based samples and their electrical properties.

3.1. XRD

X-ray diffraction (Rigaku, D/Max, 2500 V, Cu-Kα radiation: λ = 1.54056 Å) experiments were carried out on both the plain GE and the GE composite samples. Wide-angle X-ray diffractograms were recorded at temperature of 30˚C after isothermal crystallization at this temperature for 1 h.

3.2. IR Spectra

The Fourier transform infrared (FTIR) spectra were recorded on a Nicolet 8700 spectrometer, in the spectral range 400 - 4000 cm^{-1}.

3.3. TEM

TEM experiments were performed on a Hitachi H-8100 electron microscope with an acceleration voltage of 200 kV.

3.4. TGA

Thermo gravimetric analysis (TGA) was conducted on a TA instrument TGA/SDTA851 at 20 μC/min heating rate under nitrogen.

3.5. CV

All electrochemical tests were done in a three electrode CV system. The working electrode was prepared by

casting a nafion-impregnated sample onto a glassy carbon electrode. Platinum wire and a saturated calomel electrode were then used as counter and reference electrodes, respectively. The measurements were carried out in 1 M H_2SO_4 electrolyte. Electrochemical measurements were performed in an Iviumstat (Ivium Technologies).

4. Results and Discussions

4.1. XRD

In **Figure 2**, the XRD pattern of chitosan exhibits broad diffraction peaks at $2\theta = 18^\circ$ and 25° which are typical fingerprints of semi-crystalline chitosan. Graphene exhibits a strong and sharp peak at 32°, indicating a higher ordered structure. The CH-PAA showed a crystalline area in the region of $2\theta = 23^\circ, 40^\circ, 52^\circ, 61^\circ, 73^\circ$ due to the grafting of PAA onto the chitosan backbone, while XRD of the chitosan showed crystalline pattern. However, the XRD patterns of GE-CH-PAA showed peaks at $2\theta = 22^\circ, 32^\circ, 40^\circ, 53^\circ, 58^\circ, 62^\circ$ and 75° due to CH-PAA along with the GE. The increase in ordering of polymer composite with the addition of PAA indicates that the structure of GE is strongly influenced and crystalline [33]-[35].

4.2. FTIR

As shown in **Figure 3(a)**, **Figure 3(b)**, FTIR spectrum of chitosan showed a broad absorption band between 3500 cm^{-1} and 2500 cm^{-1}, centred at 3200 cm^{-1}, due to O-H stretching vibration, N-H extension vibration and the intermolecular H-bonds of the polysaccharide moieties. A band at 2790 cm^{-1} was observed corresponding to the axial stretching of C-H- bonds. A dip in transmittance at 1673 cm^{-1} was observed which is attributed to the axial stretching of C=O bonds of the acetamide group which indicated that sample was not fully acetylated. A band at 1559 cm^{-1} was observed, which is attributed to the angular deformation of the N-H bonds of the amino group. A band at 1372 cm^{-1} due to the symmetrical angular deformation of CH_3 and the amide III band at 1322 cm^{-1} were observed. The band corresponding to the polysaccharide skeleton, including vibrations of the glycoside bonds, C-O and C-O-C stretching in range 1156 - 800 cm^{-1}, were observed [36].

The FTIR dip of GE shows that O-H stretching vibrations observed at 3300 cm^{-1} was significantly reduced due to deoxygenation. However, stretching vibrations from C=O at 1735 cm^{-1} were still observed and C-O stretching vibrations at 1160 cm^{-1} became sharper, which were caused by remaining carboxyl groups. The functionalized GE (F-GE) shows dips at 3447 cm^{-1}, 2894 cm^{-1}, 1692 cm^{-1}, 1385 cm^{-1}, 1110 cm^{-1}, 891 cm^{-1}, 615 cm^{-1}. The detector observes changes in the infrared radiation, and the amplifier improves the detector signal.

The dominant dips at ~3432, ~2885, and 1700 - 1600 cm^{-1} correspond to a stretching vibration from -OH or COOH, CH_3, and C=O, respectively, demonstrating the presence of functional groups on the original GE-CH sheets. Dips at ~1700 and ~1620 cm^{-1} may be assigned to the C=O stretching vibration in COOH and in quinone functional groups as found in functional GE. The dip at ~1250 cm^{-1} is consistent with C-N stretching vibrations [37].

The amide I (1655 cm^{-1}) and amide II (1590 cm^{-1}) for GE-CH-PAA are further shifted to higher frequency 1658 cm^{-1} and 1564 cm^{-1}. Meanwhile, an OH group band at 3395 cm^{-1} in CH is also shifted towards high frequency. This result indicates an enhanced hydrogen-bonding interaction between chitosan-PAA and GE.

4.3. TEM

TEM was employed to evaluate the morphological characteristics of membranes of F-GE-CH, F-GE-CH-PAA in **Figure 4**. In **Figure 4(a)**, many obvious wrinkles and grooves are observed in GE cross-linked nanocomposite membranes compared with that of pure CH membrane, and the fracture surfaces become rougher with the increase of GE loading. This kind of cross-section morphology indicates that the tougher properties of CH cross-linked by GE. Furthermore, transmission electron microscopy (TEM) image shown in **Figure 4(b)** demonstrates the information about homogeneity and the excellent dispersion of GE in chitosan-PAA matrix. This phenomenon proves that there is the strong interaction generated by cross-linking and chain entangling of CH in the fracture areas, which should affect the mechanical properties of membranes [38].

4.4. TGA

The thermal stability of chitosan and its derivatives was analyzed using thermogravimetric analysis (TGA). The attachment of PAA to chitosan and GE-chitosan is quite evident as the weight losses are increasingly noticeable

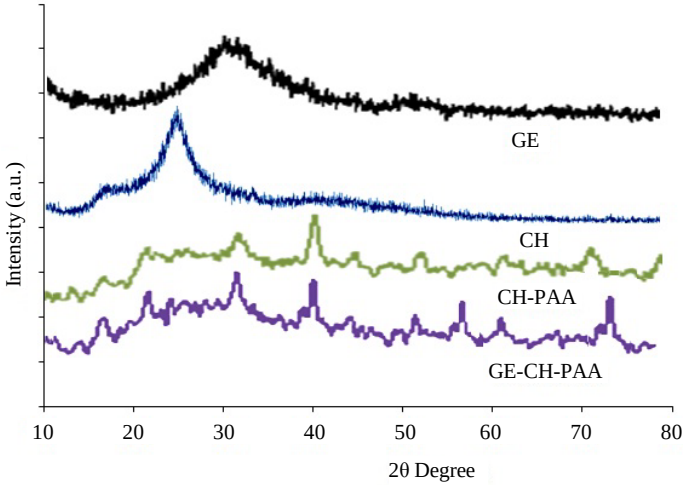

Figure 2. X-ray diffraction patterns of GE, CH, CH-PAA, and GE-CH-PAA.

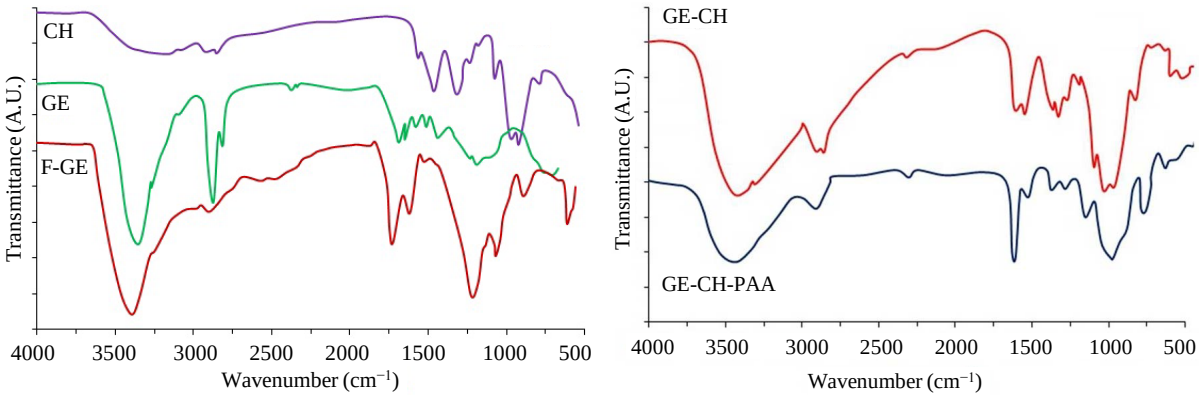

Figure 3. FTIR spectra for (a) CH, GE and F-GE, (b) GE-CH and GE-CH-PAA.

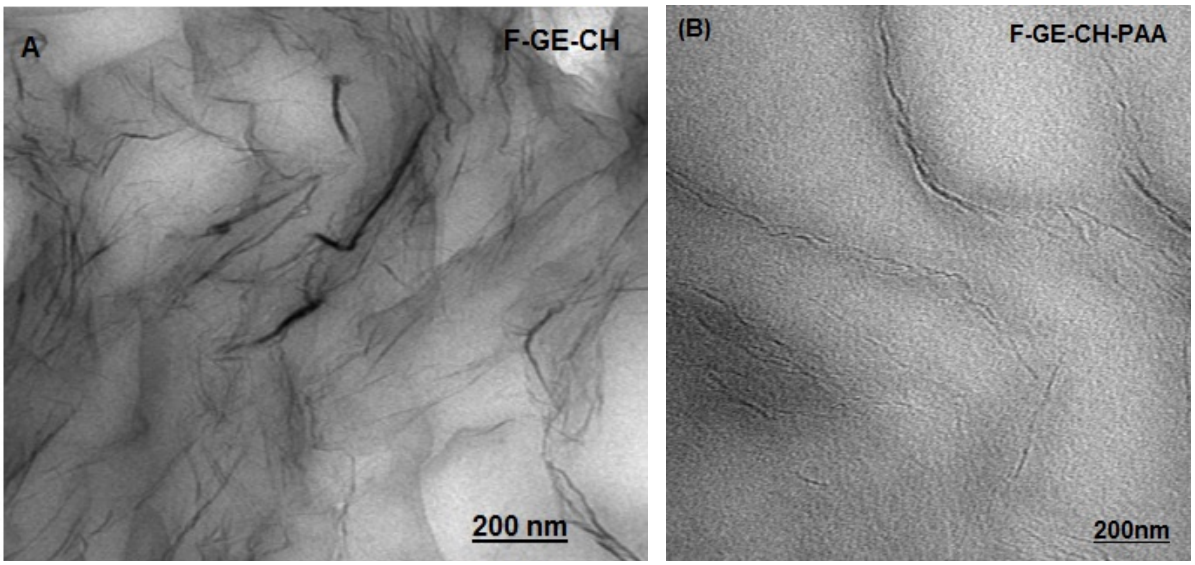

Figure 4. TEM micrographs of (a) F-GE-CH and (b) F-GE-CH-PAA nanocomposites.

(**Figure 5**). In the scan, chitosan starts to degrade near 250˚C. This is attributed to the degradation and deacetylation of chitosan [39]. Water evaporation occurred in all scans of chitosan derivative near 80˚C and is in agreement with the literature. A rapid degradation is observed for GE-chitosan-PAA derivative near 550˚C which was attributed to the presence of silyl groups of the hybrid derivative. The presence of one endotherm for all peaks indicated that all samples were homogeneous.

4.5. Cycle Voltammeter

The specific capacitances of the prepared composites with different weight ratios of PAA are presented in **Figure 6(a)**. With the introduction of GE-CH into PAA, the PAA/GE-CH composites showed improved capacitance compared to that of PAA. In particular, the GE-CH-PAA composite having 30 wt% aniline content showed the highest capacitance among the prepared samples and it presented a maximum specific capacitance of 535 Fg^{-1} at 10 $mV \cdot s^{-1}$. **Figure 6(b)** shows the cyclic voltammograms of the GE-CH-PAA composites as a function of aniline content. They show mixed behavior of electric double layer capacitance by the GE-CH component and redox (or faradaic) capacitance by the PAA. These enhanced specific capacitances are due to the GE-CH, which provided a large number of active sites and high conductivity. Beyond 50 wt% PAA content, the composite showed slightly decreased capacitance values. It is thought that PAA content over 50 wt% would produce an excessively thick coating of PAA onto GE-CH. Such a thick PAA coating could not provide effective surface

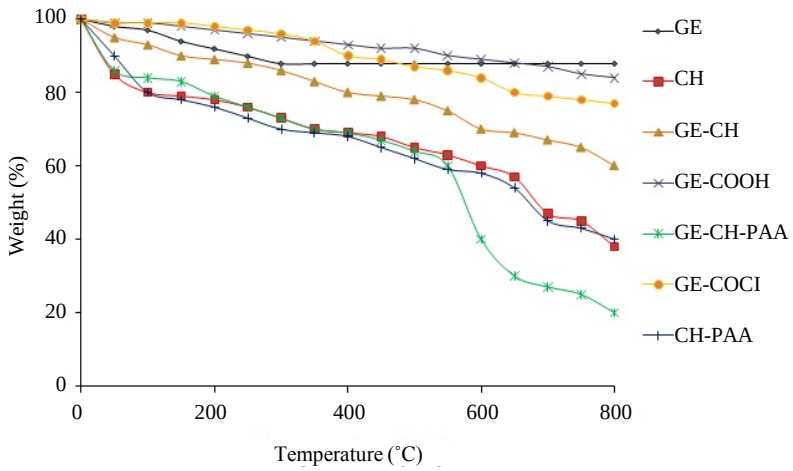

Figure 5. TGA curves for chitosan and its GE derivatives.

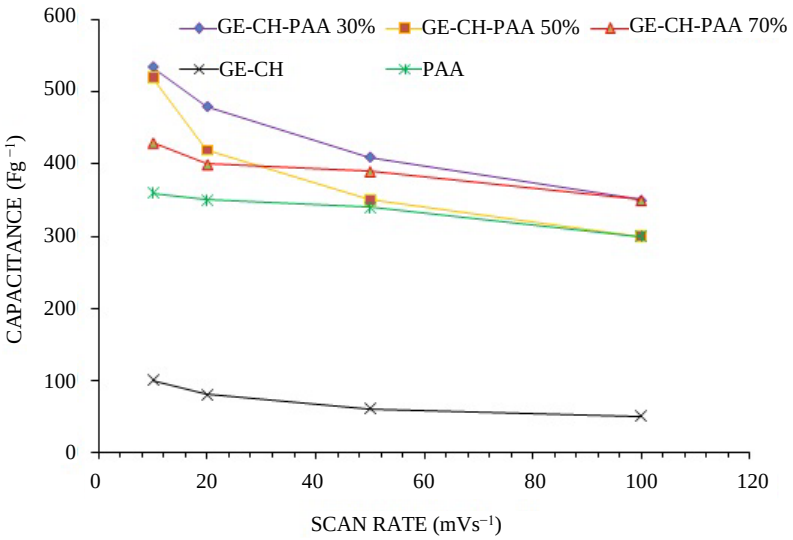

(a)

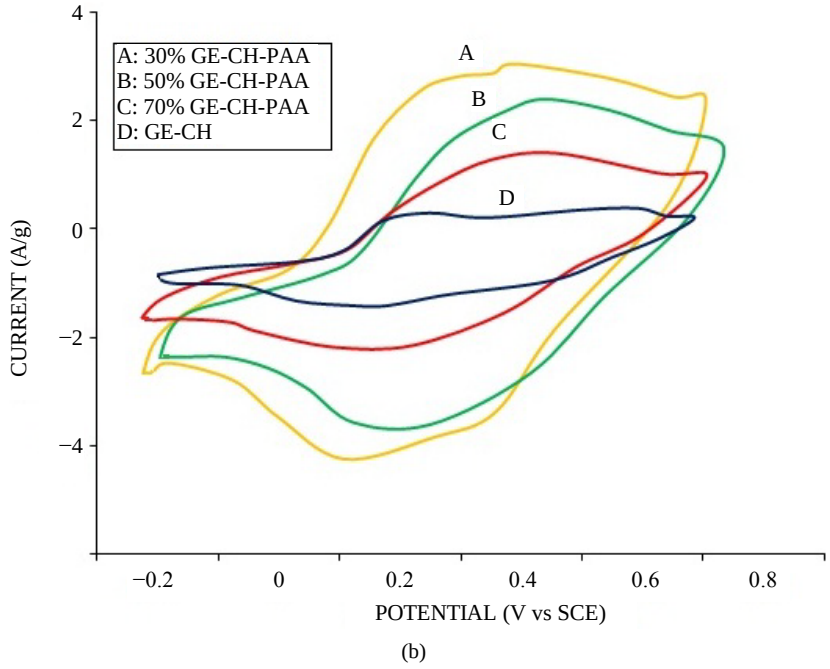

(b)

Figure 6. (a) Specific capacitance of the prepared composites at different scan rates from 10 to 100 $mV \cdot s^{-1}$; (b) Cyclic voltammetry curves of the prepared composites with different weight ratios of aniline at a scan rate of 10 $mV \cdot s^{-1}$.

area or a suitable pore structure for easy charge transfer and ion transport. Also, it was observed in **Figure 6(a)** that the specific capacitance decreases as the scan rates were increased from 10 to 100 $mV \cdot s^{-1}$. At a high scan rate, the diffusion of electrolyte ions was limited by structural properties and only the outer active surface could be utilized for charge storage.

5. Conclusion

GE-CH-PAA nanocomposites have been successfully prepared. FTIR spectra, XRD patterns and TEM images of GE-CH-PAA nanocomposites indicate the interactions existing between GE, CH and PAA. Due to this synergistic effect of PAA and nano-dimension of GE-CH-PAA, such nanocomposites can be useful as soft electromagnetic materials in constructing transformers, cathode materials in batteries and for electronic devices.

Acknowledgements

The authors would like to thank the personnel who performed XRD, TEM and TGA analysis of the sample.

References

[1] Brodie, B.C. (1859) On the Atomic Weight of Graphite. *Philosophical Transactions of the Royal Society of London*, **149**, 249-259. http://dx.doi.org/10.1098/rstl.1859.0013

[2] Brunauer, S., Emmett, P.H. and Teller, E. (1938) Adsorption of Gases from Multimolecular Layers. *Journal of the American Chemical Society*, **60**, 309-319. http://dx.doi.org/10.1021/ja01269a023

[3] Brune, D.A. and Bicerano, J. (2001) Micromechanics of Nanocomposites: Comparison of Tensile and Compressive Elastic Moduli, and Prediction of Effects of Incomplete Exfoliation and Imperfect Alignment on Modulus. *Polymer*, **43**, 369-387. http://dx.doi.org/10.1016/S0032-3861(01)00543-2

[4] Bryning, M.B., Islam, M.F., Kikkawa, J.M. and Yodh, A.G. (2005) Very Low Conductivity Threshold in Bulk Isotropic Single Wall Carbon Nanotube Epoxy Composites. *Advanced Materials*, **17**, 1186-1191. http://dx.doi.org/10.1002/adma.200401649

[5] Buchner, S., Wiswe, D. and Zachmann, H.G. (1989) Kinetics of Crystallization and Melting Behaviour of Poly(Ethylene Naphthalene-2,6-Dicarboxylate). *Polymer*, **30**, 480-488. http://dx.doi.org/10.1016/0032-3861(89)90018-9

[6] Carr, K.E. (1970) Intercalation and Oxidation Effects on Graphite of a Mixture of Sulphuric and Nitric Acids. *Carbon*, **8**, 155-166. http://dx.doi.org/10.1016/0008-6223(70)90110-7

[7] Celzard, A., McRae, E., Deleuze, C., Dufort, M., Furdin, G. and Mareche, J.F. (1996) Critical Concentration in Percolating Systems Containing a High-Aspect-Ratio Filler. *Physical Review B*: *Condensed Matter*, **53**, 6209-6214. http://dx.doi.org/10.1103/PhysRevB.53.6209

[8] Chavarria, F. and Paul, D.R. (2006) Morphology and Properties of Thermoplastic Polyurethane Nanocomposites: Effect of Organoclay Structure. *Polymer*, **47**, 7760-7773. http://dx.doi.org/10.1016/j.polymer.2006.08.067

[9] Chen, G., Wu, D., Weng, W. and Wu, C. (2003) Exfoliation of Graphite Flake and Its Nanocomposites. *Carbon*, **41**, 619-621. http://dx.doi.org/10.1016/S0008-6223(02)00409-8

[10] Cho, J.W. and Paul, D.R. (2000) Nylon 6 Nanocomposites by Melt Compounding. *Polymer*, **42**, 1083-1094. http://dx.doi.org/10.1016/S0032-3861(00)00380-3

[11] Cho, J., Luo, J.J. and Daniel, I.M. (2007) Mechanical Characterization of Graphite/Epoxy Nanocomposites by Multi-Scale Analysis. *Composites Science and Technology*, **67**, 2399-2407. http://dx.doi.org/10.1016/j.compscitech.2007.01.006

[12] Choi, E.S., Brooks, J.S., Eaton, D.L., Al-Haik, M.S., Hussaini, M.Y., Garmestani, H., Li, D. and Dahmen, K.J. (2003) Enhancement of Thermal and Electrical Properties of Carbon Nanotube Polymer Composites by Magnetic Field Processing. *Journal of Applied Physics*, **94**, 6034-6039. http://dx.doi.org/10.1063/1.1616638

[13] Chow, T.S. *(*1978) Effect of Particle Shape at Finite Concentration on Thermal Expansion of Filled Polymers. *Journal of Polymer Science Part B*: *Polymer Physics*, **16**, 967-970.

[14] Chung, D.D.L. (1987) Exfoliation of Graphite. *Journal of Materials Science*, **22**, 4190-4198. http://dx.doi.org/10.1007/BF01132008

[15] Seymour, R.W., Estes, G.M. and Cooper, S.L. (1970) Infrared Studies of Segmented Polyurethan Elastomers. I. Hydrogen Bonding. *Macromolecules*, **3**, 579-583. http://dx.doi.org/10.1021/ma60017a021

[16] Cox, W.P. and Merz, E.H. (1958) Correlation of Dynamic and Steady Flow Viscosities. *Journal of Polymer Science*, **28**, 619-622. http://dx.doi.org/10.1002/pol.1958.1202811812

[17] Cussler, E.L. (1997) Diffusion: Mass Transfer in Fluid Systems. 2nd Edition, Cambridge University Press, Cambridge.

[18] Cussler, E.L., Hughes, S.E., Ward III, W.J. and Aris, R. (1988) Barrier Membranes. *Journal of Materials Science*, **38**, 161-174. http://dx.doi.org/10.1016/S0376-7388(00)80877-7

[19] Sun, Y., Wu, Q. and Shi, G. (2011) Graphene Based New Energy Materials. *Energy Environmental Science*, **4**, 1113-1132. http://dx.doi.org/10.1039/c0ee00683a

[20] Martin, P. (2011) Graphene-Based Nanomaterials for Energy Storage. *Energy Environmental Science*, **4**, 668-674. http://dx.doi.org/10.1039/c0ee00295j

[21] Wang, H., Hao, Q., Yang, X., Lu, L. and Wang, X. (2009) Graphene Oxide Doped Polyaniline for Supercapacitors. *Electrochemistry Communications*, **11**, 1158-1161. http://dx.doi.org/10.1016/j.elecom.2009.03.036

[22] Lin, Y.C. and Chiu, P.W. (2014) Chapter 11: Effect of Adsorbents on Electronic Transport in Graphene. In: Skakalova, V. and Kaiser, A., *Graphene—Properties*, *Preparation*, *Characterization and Devices*, Woodhead Publishing, Sawston, 265-291.

[23] Deng, W., Sun, Y., Su, Q., Xie, E. and Lan, W. (2014) Porous CoO Nanobundles Composited with 3D Graphene Foams for Supercapacitors Electrodes. *Materials Letters*, **137**, 124-127. http://dx.doi.org/10.1016/j.matlet.2014.08.154

[24] Zhang, X., Han, S., Fan, C., Li, L. and Zhang, W. (2015) Hard Carbon Enveloped with Graphene Networks as Lithium Ion Battery Anode. *Materials Letters*, **138**, 259-261. http://dx.doi.org/10.1016/j.matlet.2014.10.023

[25] Patel, M.U.M., Luong, N.D., Seppala, J., Tchernychova, E. and Dominko, R. (2014) Low Surface Area Graphene/Cellulose Composite as a Host Matrix for Lithium Sulphur Batteries. *Journal of Power Sources*, **254**, 55-61. http://dx.doi.org/10.1016/j.jpowsour.2013.12.081

[26] Alves, N.M. and Mano, J.F. (2008) Chitosan Derivatives Obtained by Chemical Modifications for Biomedical and Environmental Applications. *International Journal of Biological Macromolecules*, **43**, 401-414. http://dx.doi.org/10.1016/j.ijbiomac.2008.09.007

[27] Kumar, S., Dutta, J. and Dutta, P.K. (2009) Preparation and Characterization of N-Heterocyclic Chitosan Derivative Based Gels for Biomedical Applications. *International Journal of Biological Macromolecules*, **45**, 330-337. http://dx.doi.org/10.1016/j.ijbiomac.2009.08.002

[28] Raimonda, C., Romualdas, T., Gediminas, N., Vitas, S., Gediminas, R., Zivile, R. and Rasa, P. (2014) Influence of the Laser Irradiation on the Electrochemical and Spectroscopic Peculiarities of Graphene-Chitosan Composite Film. *Electrochimica Acta*, **132**, 265-276. http://dx.doi.org/10.1016/j.electacta.2014.03.137

[29] Kumar, S. and Koh, J. (2014) Physiochemical and Optical Properties of Chitosan Based Graphene Oxide Bionanocomposite. *International Journal of Biological Macromolecules*, **70**, 559-564. http://dx.doi.org/10.1016/j.ijbiomac.2014.07.019

[30] Ryu, H.J., Mahapatra, S.S., Yadav, S.K. and Cho, J.W. (2013) Synthesis of Click-Ccoupled Graphene Sheet with Chitosan: Effective Exfoliation and Enhanced Properties of Their Nanocomposites. *European Polymer Journal*, **49**, 2627-2634. http://dx.doi.org/10.1016/j.eurpolymj.2013.06.005

[31] Viatcheslav, J. and Jacques, S. (2014) Efficient Cathodic Carboxylation of Graphene: Building a New Versatile Material. *Electrochemistry Communications*, **43**, 67-70. http://dx.doi.org/10.1016/j.elecom.2014.03.013

[32] Li, L., Luo, C., Li, X., Duan, H. and Wang, X. (2014) Preparation of Magnetic Ionic Liquid/Chitosan/Graphene Oxide Composite and Application for Water Treatment. *International Journal of Biological Macromolecules*, **66**, 172-178. http://dx.doi.org/10.1016/j.ijbiomac.2014.02.031

[33] Kumar, S. and Koh, J. (2014) Physiochemical and Optical Properties of Chitosan Based Graphene Oxide Bionanocomposite. *International Journal of Biological Macromolecules*, **70**, 559-564. http://dx.doi.org/10.1016/j.ijbiomac.2014.07.019

[34] Fan, L., Luo, C., Li, X., Lu, F., Qiu, H. and Sun, M. (2012) Fabrication of Novel Magnetic Chitosan Grafted with Graphene Oxide to Enhance Adsorption Properties for Methyl Blue. *Journal of Hazardous Materials*, **215-216**, 272-279. http://dx.doi.org/10.1016/j.jhazmat.2012.02.068

[35] Lv, J., Zhou, Q., Liu, G., Gao, D. and Wang, C. (2014) Preparation and Properties of Polyester Fabrics Grafted with O-Carboxymethyl Chitosan. *Carbohydrate Polymers*, **113**, 344-352. http://dx.doi.org/10.1016/j.carbpol.2014.06.088

[36] Sheshmani, S. and Fashapoyeh, M.A. (2013) Suitable Chemical Methods for Preparation of Graphene Oxide, Graphene and Surface Functionalized Graphene Nanosheets. *Acta Chimica Slovenica*, **60**, 813-825.

[37] Boothroyd, C.B., Moreno, M.S., Duchamp, M., Kovacs, A., Monge, N., Morales, G.M., Barbero, C.A. and Dunin-Borkowski, R.E. (2014) Atomic Resolution Imaging and Spectroscopy of Barium Atoms and Functional Groups on Graphene Oxide. *Ultramicroscopy*, **145**, 66-73. http://dx.doi.org/10.1016/j.ultramic.2014.03.004

[38] Aldosari, M.A., Othman, A.A. and Alsharaeh, E.H. (2013) Synthesis and Characterization of the *in Situ* Bulk Polymerization of PMMA Containing Grapheme Sheets Using Microwave Irradiation. *Molecules*, **18**, 3152-3167. http://dx.doi.org/10.3390/molecules18033152

[39] Srivastava, R.K., Xingjue, W., Kumar, V., Srivastava, A. and Singh, V.N. (2014) Synthesis of Benzimidazole-Grafted Graphene Oxide/Multi-Walled Carbon Nanotubes Composite for Super Capacitance Application. *Journal of Alloys and Compounds*, **612**, 343-348. http://dx.doi.org/10.1016/j.jallcom.2014.05.214